CrossMark

RESEARCH PAPER

Lattice-Preferred orientations of olivine in subducting oceanic lithosphere derived from the observed seismic anisotropies in double seismic zones

Peng Han · Dongping Wei · Keliang Zhang · Zhentian Sun · Xiaoya Zhou

Abstract Subduction zones can generally be classified into Mariana type and Chilean type depending on plate ages, plate thicknesses, subduction angles, back-arc deformation patterns, etc. The double seismic zones (DSZs) in subduction zones are mainly divided into type I and type II which, respectively, correspond to the Mariana type and Chilean type in most cases. Seismic anisotropy is an important parameter characterizing the geophysical features of the lithosphere, including the subduction zones, and can be described by the two parameters of delay time δt and fast wave polarization direction ϕ. We totally collected 524 seismic anisotropy data records from 24 DSZs and analyzed the statistical correlations between seismic anisotropy and the related physical parameters of DSZs. Our statistical analysis demonstrated that the fast wave polarization directions are parallel to the trench strike with no more than 30° for most type I DSZs, while being nearly perpendicular to the trench strike for type II DSZs. We also calculated roughly linear correlations that the delay time δt increases with dip angles but decreases with subduction rates. A linear equation was summarized to describe the strong correlation between DSZ's subduction angle α_{DSZ} and seismic anisotropy in subduction zones. These results suggest that the anisotropic structure of the subducting lithosphere can be described as a possible equivalent crystal similar to the olivine crystal with three mutually orthogonal polarization axes, of which the longest and the second axes are nearly along the trench-perpendicular and trench-parallel directions, respectively.

Keywords Seismic anisotropy · Double seismic zones · Subduction zone processes · Plate motions · Microstructures

P. Han · D. Wei (✉) · X. Zhou
Key Laboratory of Computational Geodynamics, Chinese Academy of Sciences, Beijing 100049, China
e-mail: dongping@ucas.ac.cn

P. Han · D. Wei · X. Zhou
College of Earth Science, University of Chinese Academy of Sciences, Beijing 100049, China

K. Zhang
State Key Laboratory of Earthquake Dynamics, Institute of Geology, China Earthquake Administration, Beijing 100029, China

Z. Sun
Beijing Geotherm Research Institute, Beijing 100143, China

1 Introduction

Seismic anisotropy observations can provide useful information about the Earth's interior, such as the material properties and movement patterns, which reflects its inner dynamic processes (Teng et al. 2012). With regard to seismic anisotropy in subduction zones, the geometric relationship between the fast wave polarization direction and the trench strike can be categorized into parallel, oblique, and perpendicular. Ando et al. (1983) were the first to release shear wave splitting data of subduction zones in Honshu, Japan. Since then, various scholars have conducted a series of systematic research on seismic anisotropy in subduction zones. Long and Silver (2008) and Long and Becker (2010) summarized the characteristics of seismic anisotropy for most of the world's subduction zones. Seismic anisotropy in subduction zones mainly

Springer

describes the shear wave splitting characteristics of the mantle wedge and mantle beneath the slab. The shear wave splitting characteristics of the mantle wedge are relatively complex, while the fast wave polarization directions of the subslab mantle are mostly parallel to the trench strike (e.g., Long 2013). Long and Silver (2009a, b) compiled shear wave splitting data of 15 subduction zones from previously published literatures and found that only trench migration rate correlates well with the strength of subslab anisotropy in a Pacific hotspot reference frame.

The lattice-preferred orientation (LPO) of olivine, which is the main mineral in the upper mantle, is often considered to explain the seismic anisotropy in subduction zones (e.g., Long and Silver 2008). However, a recent study indicates that hydrated products of peridotite, serpentine, with high anisotropy (about 40 % for v_P and 50 % for v_S) (Bezacier et al. 2010), may have more important influence on shear wave splitting of subduction zones. Different seismic splitting behavior can simply be inferred from two topotactic relationships between serpentine and olivine (Boudier et al. 2010). Alternative to the complex mixing minerals model of subduction zones, we propose a "pure" crystal model for explaining the fast wave polarization (see Sect. 6.4 for the details).

Subduction zones are the most seismically active areas in the Earth's surface. The frequent occurrence of earthquakes offers a favorable opportunity for exploring seismic anisotropy in subduction zones. Sykes (1966) discovered the stratified phenomena for earthquakes occurring in the Kuril Islands subduction zones. With the abundance of seismic data and the continuous improvement of earthquake location accuracy, two distinct layers were found from shallow to intermediate and deep earthquakes in global subduction zones, which are known as double seismic zones (DSZs). Kao and Rau (1999) further subdivided DSZs into type I and type II according to the morphological characteristics and focal mechanism of their subducting slabs. Even a triple-layered seismic zone exists in some subduction zones, such as northeastern Japan subduction zone (Kawakatsu and Seno 1983; Igarashi et al. 2001). A significant difference has been found in the stress characteristics of different DSZ types, and this phenomenon is attributed to the dehydration of minerals in subducting slabs (Peacock 2001; Hacker et al. 2003). Recent studies showed that DSZs type is closely related to the temperature and stress field of the subducting plate and other factors (Peacock 2001; Zhang and Wei 2008; Zhang 2010). Similarly, seismic anisotropy in subduction zones is also affected by water content, temperature, and stress characteristics.

Except for some previous studies about identification, classification, and mechanism of DSZs (e.g., Kao and Rau 1999), there were increasing researchers focusing on the seismic anisotropy in subduction zones (e.g., Fouch and Fischer 1996; Polet et al. 2000; Hammond et al. 2010). Song and Kawakatsu (2012) found that fast wave polarization direction changes from trench-parallel under relatively steep subduction zones to trench-normal under shallow subduction zones. Long (2013) provided a detailed review of the subduction geodynamics from seismic anisotropy. Our study is more concerned about the seismic anisotropy within DSZs. With regard to DSZs, the scope of the study area is smaller, the type is clear, and more detailed features of subduction zones can be reflected. Moreover, DSZs widely distributed in the global subduction zones (Brudzinski et al. 2007; Zhang and Wei 2011) can reflect not only local characteristics of subduction zones, but also the general characteristics. Different types of DSZs have different slab stress states, so they represent different subduction condition, such as temperature, pressure, water content, etc. Therefore, we could have insights into subduction process through the exploration of seismic anisotropy in DSZs. In this paper, we collected both seismic anisotropy data and the related parameters of DSZs in subduction zones and statistically analyzed the relationship between seismic anisotropy in subduction zones and the type of DSZs. We attempted to find correlations between them and then used Fresnel polarization ellipsoid to discuss their geodynamical implications and physical mechanism.

2 Subduction zones and DSZs

Global subduction zones are mainly classified into Mariana type and Chilean type depending on subduction angles, oceanic plate age, plate thickness, back-arc deformation pattern, and so on (Uyeda and Kanamori 1979; Stern 2002). Mariana-type subduction zones have large subduction angle and strong extension in back-arc, whereas Chilean-type subduction zones have small subduction angle and strong compression in back-arc. By combining previous research results and the stress states of the global earthquake catalogs, DSZs can be roughly divided into two categories: type I or type II DSZs, which are described by the subduction angles α_s and α_d, respectively (Kawakatsu 1986a; Kao and Rau 1999; Fig. 1). See Sect. 5.1 for details.

Type I DSZs are characterized by the down-dip compression (DDC) and down-dip tension (DDT) of the upper and lower layers, respectively. The layer separation (L) is approximately 20 km to 40 km. This separation decreases with subduction depth and converges fully at 200 km (Hasegawa et al. 1978, 1994). DSZs belonging to this type are mainly distributed in the subduction zones of Kuril-Kamchatka Island arc, Kanto in Japan, northeastern Honshu in Japan, Mariana, and Tonga. Unbending properties are believed to produce this type of DSZ (Kawakatsu
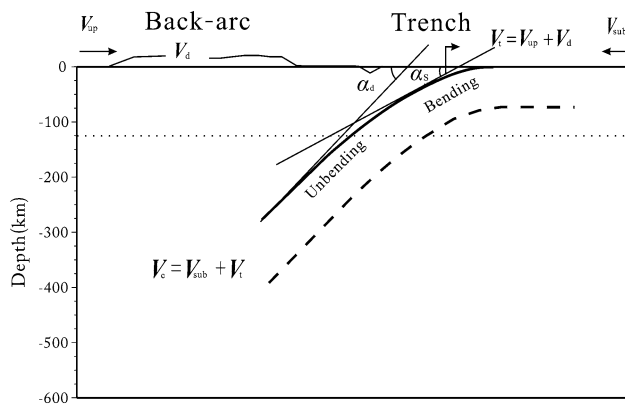
Fig. 1 Schematic of subduction zones and subduction parameters (after Kawakatsu 1986b; Lallemand et al. 2005). V_{sub} is the absolute velocity of the subducting plate, V_t is the trench migration velocity, V_{up} is the overriding plate velocity, V_d is the deformation rate in the back-arc region, V_c is the convergence velocity, α_s is the shallow dip angle, and α_d is the deep dip angle

1986b); the slab bends downward during subduction and causes tensile stress to the convex plate. With the increase of subduction depth, the plate becomes straighter and is divided into DDC and DDT stress states by the neutral surface. Deep earthquakes are strongly influenced by temperature and subduction parameters. Other factors may also lead to the formation of deep earthquake DSZs.

Type II DSZs are characterized by a shallow focus depth and smaller layer separation (typically less than 15 km) with the same stress state. Layer separation converges at about 150 km depth and is often accompanied by lateral compression and DDT. The DSZs in the subduction zones of New Zealand's North Island, northern Chile, northeastern Taiwan, Cascadia, Cook Inlet in Alaska, and New Britain mostly belong to this type (Kao and Rau 1999; Hacker et al. 2003; Yamasaki and Seno 2003). Mineral dehydration can cause changes in pore pressure, leading to a brittle fracture that can result in earthquakes. Dehydration is primarily concentrated in areas above 150 km, which might explain type II DSZs. However, an accurate earthquake location tool has revealed that earthquakes in the subduction zone of northeastern Japan are even distributed in three layers, because of the DSZ extending to a low-angle thrust seismic zone (Kawakatsu and Seno 1983).

Seismic-converted wave and refraction wave method can be employed to determine the upper and lower bounds of DSZs (Hasegawa et al. 1994; Ohmi and Hori 2000; Igarashi et al. 2001). Earthquake catalogs, moment tensors, and other tools can determine the stress state and related parameters of DSZs. Brudzinski et al. (2007) reported the unified standard distribution of 31 DSZs and their parameters were obtained by rotating source coordinates to the direction perpendicular to the subduction direction. They

found that the layer separation of DSZs is proportional to the age of the slab. The layer separation can be estimated independently by the well-known plate age (A), thus eliminating observation errors introduced by different locational accuracy and regional networks (Zhang and Wei 2011).

However, Brudzinski et al. (2007) used trench age as the overall age of the subducting slab. Actually, this age could not accurately reflect the physical properties of the subducting slab at different subduction depths. To solve this problem, Zhang and Wei (2011) added eight new DSZs, namely four from Kamchatka, two from Juan de Fuca, and two from Nazca, based on the work of Brudzinski et al. (2007). Combined with the 31 groups of DSZ parameters provided by Brudzinski et al. (2007), totally 39 groups of DSZ parameters in subduction zones were obtained in their work (Fig. 2). Zhang and Wei (2011) comprehensively discussed the relationship between DSZs and subduction geometric, kinematic, and dynamic parameters, and the nature of the overlying plate. Further study showed that the relevant subduction geometric parameters contain slab length, maximum subduction depth, shallow dip angle, and deep dip angle. The layer separation of DSZs is positively correlated with shallow and deep dip angles. The linear relationship is not obvious, and the relationship among layer separation, slab length, and maximum subduction depth is unclear. Slab age, as an independent variable, reflects the characteristics of subduction dynamics. The linear relationship between the independent variable and layer separation is $L = 0.15A + 6.55$. The observations will be flattened when the plate age is greater than 80 Ma. Considering the general case, the relationship between slab age and layer separation can be expressed as $L = 2.44A^{1/2} - 2.36$ (Zhang and Wei 2012). The layer separation of DSZs is positively correlated with absolute velocity of the subducting plate but is weakly correlated with convergence rate. This implies that the absolute velocity of the subducting plate may play an important role in DSZs.

The subducting plate of type I DSZs generally corresponds to Mariana-type slabs, and layer separation is mainly correlated with age, slab pull, and other dynamic parameters. In contrast, the subducting plate of type II DSZs corresponds mostly to Chilean-type slabs, and layer separation is not only affected by dynamic factors but also related to the local stress state. The nature of the subducting slab determines layer separation in DSZs. However, there are several exceptions within the 39 subduction zones, for example, both NZ1 and NZ2 in southern America are classified as type I DSZs, while HEB in Tonga is classified as type II DSZ, and EA2 cannot be classified as either type I or type II DSZ (Zhang and Wei 2012).
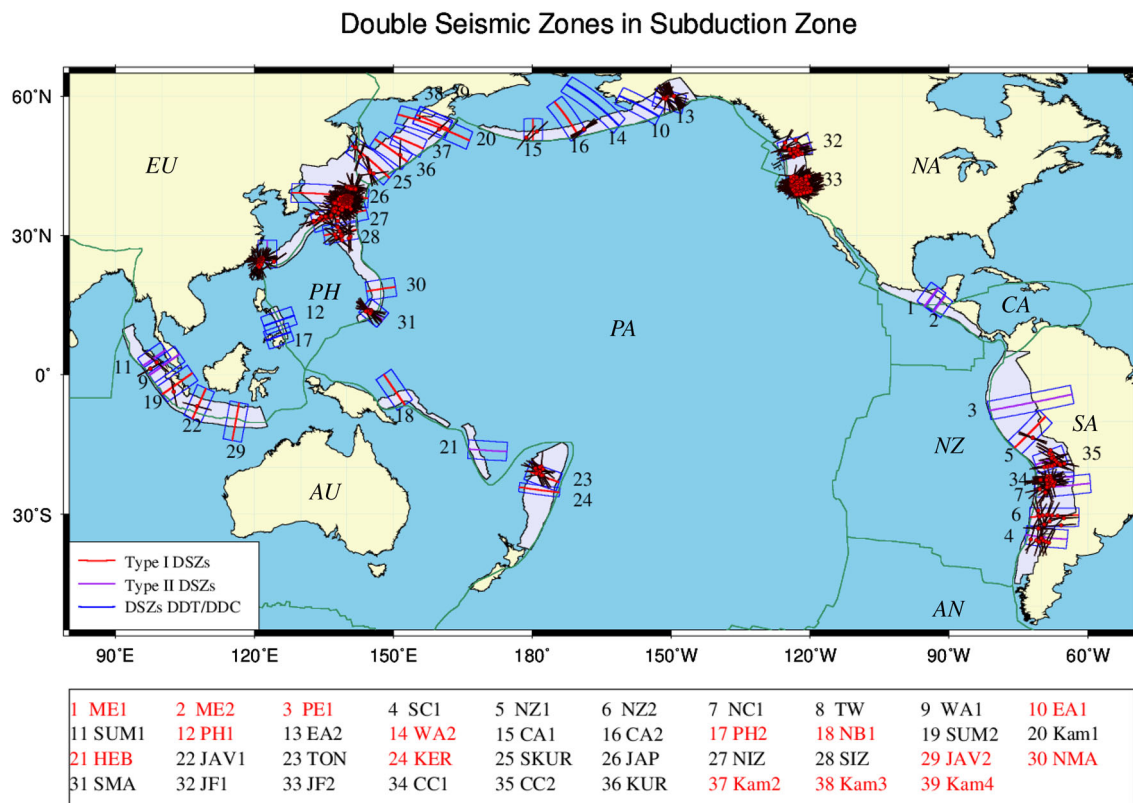
Fig. 2 Distribution of global subduction zones, DSZs, data, and research areas (refer to Zhang and Wei 2011). The *rectangles* (with *thin blue lines*) denote the research regions; the regions in *light purple* are the subduction zones. The plate abbreviations are as follows: *AN* Antarctic, *AU* Australia, *PH* Philippine Sea, *PA* Pacific, *NA* North America, *SA* South America, *NZ* Nazca, *CA* Caribbean, and *JF* Juan de Fuca. The figures are the numbers of the corresponding DSZs. The numbers correspond to the DSZs' abbreviations in the large *rectangle below* the main figure. The *red circles* represent the anisotropy data and the *lines* represent fast wave polarization direction

3 Seismic anisotropy data in subduction zones

Schutt and Fouch (2001) and Wüstefeld et al. (2009) collected and compiled seismic anisotropy data from different studies. Several researchers, including Wirth and Long (2010) and Liu et al. (2008), also discussed the quality of the data in their studies. High-quality seismic anisotropy data generally have a high signal-to-noise ratio, a clear waveform, elliptical particle motion, and linear or nearly linear corrected particles. High-quality data require agreement between the rotation-correlation method (Ando et al. 1983) and Silver and Chan's method (Silver and Chan 1991), namely $\pm 10°$ for fast wave polarization direction ϕ and ± 0.5 s for delay time δt. Fair-quality data require $\pm 20°$ for ϕ and ± 1.0 s for δt, a low-quality waveform, and less linear corrected particle motion. On this basis, Sun and Wei (2013) combined independent collections of global seismic anisotropy data from the recent literatures and obtained a total of 7959 related datasets after filtering and removing duplicate and poor-quality data. Given the fact that most of the anisotropic parameter error estimation for our collected data was not mentioned in the original

literature, see Supporting Information attached in this study or the website at http://splitting.gm.univ-montp2.fr/DB/for more detailed information.

It is somewhat difficult for us to directly extract the seismic anisotropy in subduction zones from splitting measurements. However, many previous studies demonstrated that the dominant source of seismic anisotropy appears to be from the upper mantle in the case of teleseismic P-to-S conversions (Savage 1999; Silver 1996). Both the IASP91 model and the global anisotropic structure model by Zhang (2002) showed that seismic anisotropy of the upper mantle is quite strong despite the relatively weaker anisotropy from 300 to 600 km depth (e.g., Bastowa et al. 2015). Apart from the lower transition zone (660–1000 km) and D'' layer, anisotropy of the entire lower mantle is weak (e.g., Savage 1999; Zhang 2002).

This study mainly focuses on seismic anisotropy in DSZs. The seismic anisotropy data used in this study are mostly from SKS (SKKS, PKS etc.). If there exists anisotropy between the core-mantle boundary and the receiving station, SKS wave will be splitted into two subwaves with perpendicular polarization and various

velocities. Therefore, SKS splitting could be utilized to sample the seismic anisotropy within the region between the core-mantle boundary and the receiving station (e.g., Silver and Chan 1988). Three obvious advantages of this method are as follows: (1) straightforward anisotropic observation, (2) higher tangential solution, and (3) reliable computation result and rare multiple solutions. SKS splitting has become one of the most popular research methods on the seismic anisotropy. The P-to-S wave converts at core-mantle boundary when it sequentially propagates to a station from the K-to-S wave or P-to-S wave (i.e., line segment BS in Fig. 3). Thus, delay time records the primary part of seismic anisotropy through both the mantle and crust beneath the station regions and reasonably reflects upper mantle (and crust) seismic anisotropy beneath the station areas (i.e., seismic ray path segment CS in Fig. 3) when we neglected relatively weak seismic anisotropy through the lower mantle (i.e., segment BC in Fig. 3). This is consistent with the previous studies on the global pattern of fast SKS splitting anisotropy data by Faccenda et al. (2008). They demonstrated that SKS splitting may primarily reflect seismic anisotropy in the shallow part of the slab due to aligned serpentinized cracks.

4 Oriented statistical analysis and Rayleigh test

The scope of the related subduction zone in this study was also determined according to the starting point using the rule provided by Brudzinski et al. (2007) for the determination of DSZ profiles. The profile is the center, with 2° on both sides, and the rectangular area is the research area. All study areas were obtained from 524 sets of seismic anisotropy data (see the supplementary material for details), which are mainly distributed in 24 out of 39 DSZs. The other 15 DSZs, such as the Philippine Sea DSZs (PH1,

Fig. 3 Schematic of path of the phase SKS and the anisotropic structure of the Earth, after Garnero. (http://garnero.asu.edu/research_images)

PH2) and Hebrides (HEB) DSZs, have no data. These data from the 524 sets mainly show the cited seismic anisotropy in subduction zones from SKS splitting beneath the station areas. We used the data to study the correlations with the DSZs' related parameters in subduction zones.

A geostatistical method was employed to analyze seismic anisotropy data in each subduction zone. The fast wave polarization direction is similar to stress orientation. Although it is not a vector, we can still apply a resultant vector summation method to deal with in most cases (Coblentz and Richardson 1995). Because the polarization directions are generally recorded in the range of 0° to 180°, measured clockwise from north, we use the double-angle technique suggested by Mardia (1972) to solve the inflating problem of the polarization directions. For example, the fast wave polarization direction 3° and 7° are almost the same orientation, but it represents opposite direction. If we directly use their values in the resultant vector summation, it will give the misleading result.

Spatial orientation data were initially multiplied by 2 and then scaled to a new equivalent unit vector. Their X_i and Y_i components were then obtained in X and Y coordinates, respectively, as follows:

$$X_i = \cos 2\phi_i, \quad Y_i = \sin 2\phi_i, \tag{1}$$

where $2\phi_i$ is the included angle with X coordinates for the ith equivalent unit vector. Calculating all the components of the equivalent unit vectors and summing both the sines and cosines of the individual vectors, we obtain

$$X_\Phi = \sum_{i=1}^{n} \cos 2\phi_i, \quad Y_\Phi = \sum_{i=1}^{n} \sin 2\phi_i, \tag{2}$$

where n is the sample size. Mean direction $\overline{\Phi}$, which is the angular average of all vectors in a sample, was then obtained.

As an example, fast wave polarization direction is 40°, and its orientation could equally well be recorded as 220°. If we double these angles, we obtain 80° and 440°, which also become $(440° - 360°) = 80°$ coinciding each other. To recover the true mean polarization direction ϕ in the defined subduction zones, we simply divide the calculated mean value $\overline{\Phi}$ by two (see also in Fig. 5.23 by Davis 1986).

Let the resultant length, R, be a measure of dispersion by the Pythagorean Theorem as follows:

$$R = \sqrt{X_\Phi^2 + Y_\Phi^2} = \sqrt{\left(\sum_{i=1}^{n} \cos 2\phi_i\right)^2 + \left(\sum_{i=1}^{n} \sin 2\phi_i\right)^2}. \tag{3}$$

However, the standardized resultant length is often used in actual statistical analysis and it is defined by
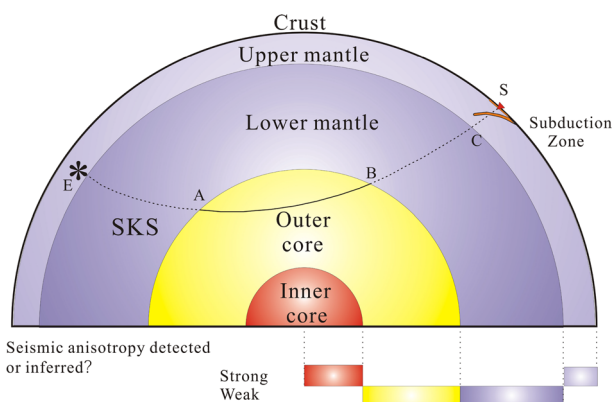
$$\bar{R} = \frac{R}{n}. \tag{4}$$

Quantity $\bar{R}$, the mean resultant length, ranges from 0 to 1 according to Eq. (4). Large values of $\bar{R}$ indicate that the observations are tightly correlated with a small dispersion. We use the Rayleigh test (Mardia 1972, Chap. 6) in this study to estimate polarization direction in subduction zones. The Rayleigh test is simple and involves only the calculation of $\bar{R}$. This statistic is compared to a critical value of $\bar{R}$ for the desired level of significance. However, if the computed statistic is so large that it exceeds the critical value (Mardia 1972), the null hypothesis must be rejected and the observations might have a preferred orientation. So, the Rayleigh test determines the subduction zones for which the null hypothesis that the polarization directions are random can be rejected. It is based on the assumption that the observations come from a von Mises distribution, which is a circular equivalent of the normal distribution (Mardia 1972). If the orientation data are sampled from other distribution, the test will display misleading results. The critical values of $\bar{R}$ for Rayleigh's test of a preferred trend at various levels of significance (i.e., 95 %, 97.5 %, or 99 %) and numbers of observations were provided by Mardia (1972). If the computed $\bar{R}$ exceeds the critical value, the null hypothesis must be rejected and a preferred polarization direction may exist in the subduction zone, which is the mean direction $\overline{\Phi}$.

Of all the 24 subduction slabs containing the 524 polarization records, only 20 slabs contain two or more polarization records that can be used in the above Rayleigh test. Five slabs including NZ2 and NIZ in Japan, SIZ in Izu-Bonin, and WA1 and SUM1 in Sumatra-Java failed the Rayleigh test at the 95 % confidence levels and were thus excluded. There are mainly two possible reasons that these 5 DSZs do not pass the Rayleigh test: (1) Measurement methods. Each of them with their own biases, assumptions, preprocessing steps, and error estimation procedures is widely used in researches. (2) Frequency diversity. Different frequency contains different useful information. For example, higher-frequency data for splitting analysis often contain information about near-surface seismic anisotropy (Long and Silver 2009a). These different sources of fast polarization data give random directional distributions, which imply the complex anisotropy patterns of the different splitting wave ray paths. We list their average polarization directions within the other 15 subduction slabs which pass the Rayleigh test (Table 1). Combining with four slabs only containing one polarization direction, 19 subduction slab zones in total with preferred polarization directions are listed in Table 1.

5 Statistical analysis of seismic anisotropy in subduction zones

5.1 Mean fast wave polarization direction and DSZs

The subduction angle is an important parameter describing a geodynamical property of DSZ. Lallemand et al. (2005) observed the major change in dip occurring at around 125 km depth. They thus defined a mean shallow dip between 0 and 125 km called α_s and a mean deep dip for depths greater than 125 km called α_d (Fig. 1). As the Mariana-type subduction zones have much larger dip angle than the Chilean-type ones, and most of the type I DSZs extend to the depth larger than 125 km, while the type II DSZs are mostly distributed shallower than 100 km, the deep angle for Mariana-type subduction zones plays a more significant role in controlling the stress state of the DSZs, and could be more feasible to describe the geometry of type I DSZs. Thus, we uniformly used a DSZ's angle called α_{DSZ} to define the subduction angle describing both type I and type II DSZs. α_{DSZ} is equal to the deep dip angle α_d for type I and the shallow dip angle α_s for type II. We excluded one subduction zone of EA2 because it belongs to a special DDT/DDC state of subducting slab and cannot be included as either type I or type II DSZs. Among the rest of the 18 subduction slab zones with preferred polarization directions listed in Table 1, 10 α_{DSZ} angles come from type I of the related DSZs and 8 α_{DSZ} angles from type II DSZs. It is worth noting that we just calculated the related parameters (e.g., average fast direction, angle between trench strike and fast direction) from the data that we collected and without considering error, but it can really reflect the general characteristics. We also listed these 18 subduction angles (α_{DSZ}) in Table 1.

Many DSZs appear to be dominated by either trench-parallel preferred fast directions (e.g., JAV1, CA2, and Kam1) or trench-perpendicular preferred fast directions (e.g., JF1, JF2, and CC1). We defined $|\phi_T - \phi|$ to describe the included angle between average fast wave polarization direction ϕ and trench strike ϕ_T. In this study, we found that the DSZ's type can be mostly classified by either its subduction angle α_{DSZ} or the $|\phi_T - \phi|$ angle (Fig. 4a, see also Table 1). In other words, if we used two lines of $\alpha_{DSZ} = 45°$ and $|\phi_T - \phi| = 45°$ to divide a square into four quadrants, we could find that type I and type II DSZs are preferably located in different quadrants, respectively. When the included angle $|\phi_T - \phi|$ is less than 45° and subduction angle α_{DSZ} is in the range of 45° to 90°, i.e., the 'fourth' quadrant, the corresponding DSZs all belong to type I. Although each of them has only one set of data for Kamchatka (Kam1), Java (JAV1), and Sumatra (SUM1) DSZs, other related researches have also shown that the polarization direction is nearly parallel to trench strike in

Table 1 Distribution of seismic anisotropy data in global subduction zones

| Subduction zone | Seismic data type | Number | DSZs' related data | | | | | $\bar{R}$ | ϕ | Rayleigh test | $\bar{\delta t}$ | $\phi_T - \phi$ | Source and references |
			Name	Type	α_{DSZ}	V_c	Number						
Kamchatka	SKS	170	Kam1	I	56	75	1	–	33.0	1	1.60	13.0	Fouch and Fischer (1996), Long and van der Hilst (2005), Iidaka and Obara (1995), Hiramatsu et al. (1997), Nakajima et al. (2006), Vinnik et al. (1992), and Barruol and Hoffmann (1999)
Kurils	SKKS		SKUR	I	40	76	9	0.680	174.9	Pass	0.59	45.8	
Japan	PKS		JAP	I	29	86	119	0.175	129.8	Pass	0.17	54.3	Vinnik et al. (1992), and Barruol and Hoffmann (1999)
			NIZ	I	31	93	40	0.194	104.2	–	0.52	61.8	
			KUR	I	47	77	1	–	1.0	1	1.80	34.0	
South America	SKS	84	SC1	II	21	66	9	0.666	14.7	Pass	0.91	8.5	Vinnik et al. (1992), Barruol and Hoffmann (1999), Anderson et al. (2004), Russo and Silver (1994, 1996), Kaneshima and Silver (1995), Meade et al. (1995), Polet et al. (2000), and Bock et al. (1998)
			NZ1	I	50	58	3	0.992	110.7	Pass	0.80	24.2	
			NZ2	I	–	69	12	0.329	24.8	–	0.95	27.1	
			NC1	II	17	71	30	0.445	62.0	Pass	0.84	67.0	
			CC1	II	18	71	13	0.871	80.9	Pass	0.85	80.9	
			CC2	II	25	63	17	0.788	100.5	Pass	0.82	59.5	
Cascadia	SKS	147	JF1	II	17	37	21	0.806	66.9	Pass	1.12	82.1	Long et al. (2009), Bostock and Cassidy (1995), Özalaybey and Savage (1995), Currie et al. (2004), Evans et al. (2006), Bonnin et al. (2010), Eakin et al. (2010), Monteiller and Chevrot (2011), West et al. (2009)
			JF2	II	16	24	126	0.692	69.6	Pass	1.44	79.5	
			WA1	II	28	28	2	0.358	94.1	–	1.29	51.1	
Sumatra-Java	SKS	6	SUM1	II	29	41	2	0.358	94.1	–	1.29	51.1	Hammond et al. (2010)
			SUM2	I	49	38	1	–	168.0	1	0.83	23.1	
			JAV1	I	68	57	1	–	105.0	1	1.89	8.9	
			EA2	DDT/DDC	–	47	31	0.820	159.0	Pass	1.02	36.5	
Alaska-Aleutians	SKS	39	CA1	I	62	59	2	0.993	29.5	Pass	1.20	60.5	Hanna and Long (2012)
			CA2	I	60	65	6	0.976	42.8	Pass	0.82	11.8	
Izu-Bonin-Marianas	SKSS	27	SIZ	I	61	51	12	0.170	105.0	–	0.90	65.0	Iidaka and Obara (1995), Anglin and Fouch (2005), Hiramatsu et al. (1997), and Fouch and Fischer (1998)
			SMA	II	40	65	15	0.856	128.3	Pass	0.27	88.6	
Kermadec-Tonga	SKS	12	TON	I	57	104	12	0.551	135.7	Pass	1.58	64.3	Bowman and Ando (1987) and Wookey et al. (2002)
Ryukyu	SKS	39	TW	II	37	51	39	0.393	33.0	Pass	1.20	57.0	Vinnik et al. (1992), Kuo-Chen et al. (2009), and Long and van der Hilst (2006)

α_{DSZ} is the subduction angle of DSZs (degree); V_c is the subduction (convergence) velocity (mm/a); $\bar{R}$ is the mean resultant length; ϕ is the mean direction; $|\phi_T - \phi|$ is the included angle between trench strike and mean direction; $\bar{\delta t}$ is mean delay time

In the column related to the Rayleigh test, "1" means one data in the DSZs, "Pass" means passing the Rayleigh test, and "–" means failing the Rayleigh test

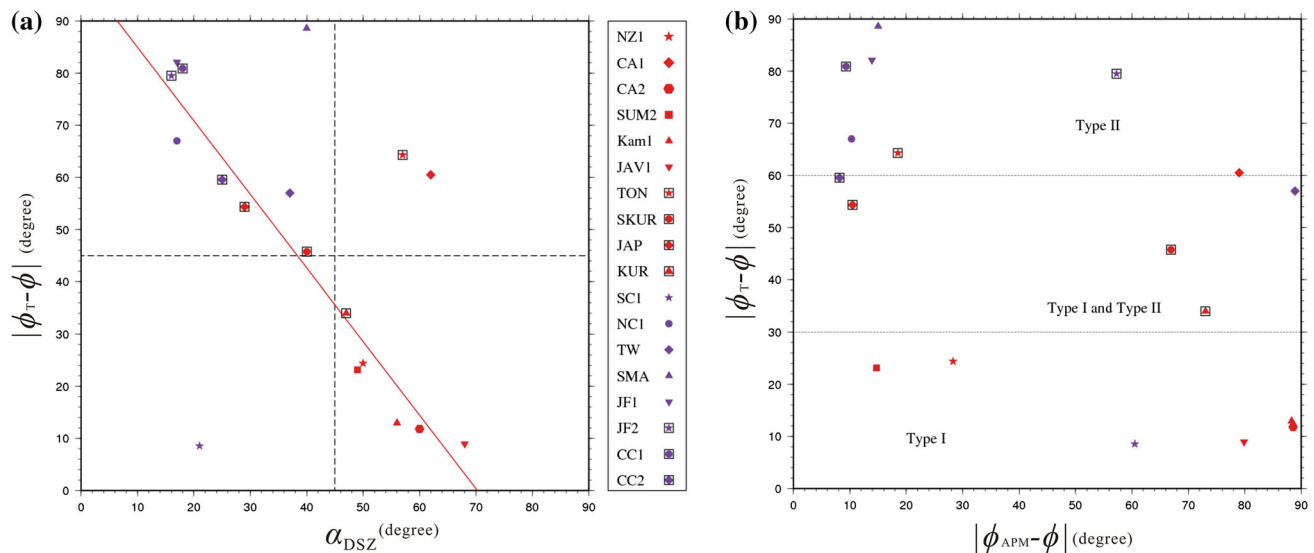Only DSZs that contain seismic anisotropy data are listed in this table. The names of the DSZs correspond to Fig. 2

Fig. 4 Relationship between anisotropy and DSZs. **a** Subduction angle of DSZs and anisotropy. **b** Relationship between average fast wave polarization direction and trench strike, APM orientation. The type I DSZs are in *red*, and the type II DSZs are in *purple*. The *red line* indicates a linear fit to the data without considering SC1, SMA, TON, and CA1. ϕ_T is the trench strike; ϕ is the average fast wave polarization direction; $|\phi_T - \phi|$ means the intervening angle between trench strike and average fast wave polarization direction

these areas (Hammond et al. 2010; Peyton et al. 2001). When subduction angle α_{DSZ} is less than 45° and included angle $|\phi_T - \phi|$ is in the range of 45° to 90°, or in the 'second' quadrant, the corresponding DSZs are mostly type II with two type I exceptions of Aleutian (CA1) and Tonga (TON) DSZs. Moreover, the included angle $|\phi_T - \phi|$ is large for two type I DSZs of TON and SKUR, which are located in the 'first' quadrant in Fig. 4a. For example, the included angle $|\phi_T - \phi|$ in the northeastern Japan (JAP) DSZ is significantly large (54.3°), which may be associated with the complexity of the trench boundary and triple junction. Regardless of the subduction orientation, the statistical results show that most of the average fast wave polarization directions of type I are parallel to trench strike or the included angle is small, whereas the average fast wave polarization direction is trench vertical or nearly vertical for type II.

We also compared DSZs' subduction angle α_{DSZ} with included angle $|\phi_T - \phi|$ (Fig. 4a). Obviously, included angle $|\phi_T - \phi|$ can be reasonably constrained in the range of 0° to 90° because either ϕ_T or ϕ is similar to the fault's strike changing from 0° to 180°, measured clockwise from north. Regression results show that the included angle $|\phi_T - \phi|$ decreases with the increase of α_{DSZ}. That is to say that the polarization direction tends to be parallel to the trench strike for large subduction angles, while being perpendicular to the trench strike for small subduction angles, which is consistent with that observed by Song and Kawakatsu (2012). Least squares method was used to obtain the linear relationship between α_{DSZ} and the

included angle without considering four DSZs including Mariana (SMA), Tonga (TON), Aleutian (CA1), and Nazca (SC1) DSZs. These four DSZs are located in the 'first' and the 'third' quadrants in Fig. 4a, and we will discuss them later. The calculated equation is as follows:

$$|\phi_T - \phi| = -1.41\alpha_{DSZ} + 99.0. \tag{5}$$

5.2 Average delay time and DSZs

The average delay time of those 19 global subduction zones with preferred polarization directions is in the range of ~0.2 s to ~1.8 s (Table 1). There are large variations in average delay times for these slab zones, with some zones exhibiting relatively weak seismic anisotropy (e.g., JAP and SMA DSZs) and some others exhibiting delay times up to ~2 s (e.g., JAV1 and KUR DSZs). This is consistent with the complex spatial variations of shear wave splitting patterns in most mantle wedges worldwide concluded by Long and Wirth (2013). The correlations of the average delay time δt with convergence rate V_c, as well with DSZ's subduction angle α_{DSZ}, were analyzed (Fig. 5). The average delay time δt in DSZs decreases gradually with the increase in the convergence rate V_c (Fig. 5a). The corresponding relationship between average delay time δt and V_c was calculated with the least squares method using the equation: $\delta t = -0.0032V_c + 1.23$. Excluding Kam1, JAV1, TW, TON, and KUR DSZs (the points in black ellipse), the linear fitting result is described using the following equation:

$$\delta t = -0.015V_c + 1.69. \tag{6}$$

The value of correlation coefficient is $R = -0.7333$ for Eq. 6, and it is small for all points, so we can use Eq. 6 to roughly describe the relationship between average delay time δt and convergence rate V_c. However, the influence of the average delay time δt is different with subduction angle. We also found a mildly linear relationship (correlation coefficient $R = 0.3753$) between DSZ's subduction angle α_{DSZ} and average delay time δt. Average delay time δt increases with DSZ's subduction angle α_{DSZ} (Fig. 5b), and the equation is as follows:

$$\delta t = 0.016\alpha_{DSZ} + 0.32. \tag{7}$$

Although we obtained an equation of DSZs' subduction angle and delay time, they can only weakly reflect the correlation between them, and it also illustrates the complexity of seismic anisotropy in subduction zones. The relationships among average delay time δt and other related DSZ's subduction parameters, including layer separation of DSZs, slab age, and maximum subduction depth, were also analyzed in this study. The results show that the relationships among average delay time and these related parameters are difficult to summarize with a linear relationship.

With regard to delay time, $\delta t = L\delta\bar{\beta}/\beta_0$, where L is the path length, β_0 is the isotropically averaged shear velocity (Silver 1996), and $\delta\bar{\beta}$ is the dimensionless intrinsic anisotropy. Delay time is obviously associated with anisotropic material and the whole ray path, and is mainly related to the spatial distribution of the anisotropic material. Nevertheless, as we mentioned in Sect. 3, the anisotropy data used in this research mainly record the seismic anisotropy properties beneath the station areas. The statistical results show that seismic anisotropy in DSZs is related to subduction rate or other slab geometrical properties. The average delay time exhibits a linear correlation with V_c and DSZ's subduction angle α_{DSZ}. This possibly reflects the complex geodynamical processing, i.e., different stress regime that corresponds to different types of DSZs in subduction zones.

6 Discussion and conclusions

6.1 Complexities of seismic anisotropy in subduction zones

Figure 4a shows that the included angle $|\phi_T - \phi|$ decreases with the increasing subduction angle α_{DSZ} of DSZ. However, there are four exceptions to this pattern including SMA in Southern Marianas, SC1 in Southern Chile, TON in Tonga, and CA1 in Central Aleutian, which are excluded from the regression line fitting (Eq. 5). There are 15 seismic anisotropy data records in SMA region and 9
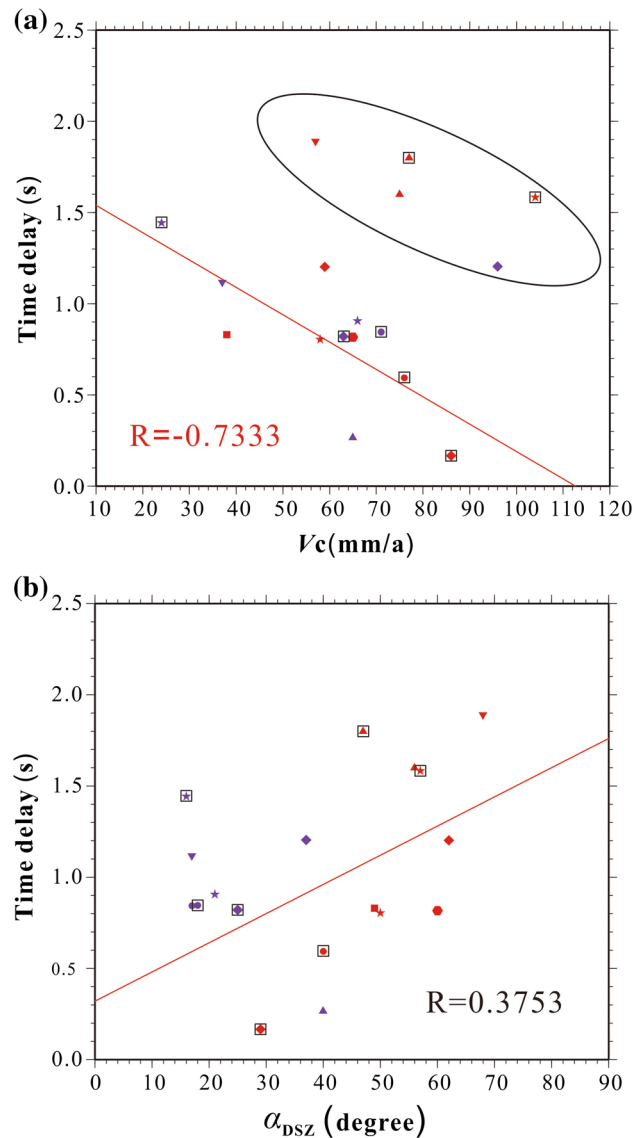

Fig. 5 Relationship between several subduction parameters and average delay time. **a** Relationship between subduction rate and average delay time. The *thin red line* indicates a linear fit to the data without considering Kam1, JAV1, TW, TON, and KUR. **b** Relationship between DSZs' angle and average delay time; the *thin red line* indicates a linear fit to all data without JF2. The meanings of the symbols are the same as in Fig. 4

anisotropy data records in SC1 (Fig. 2; Table 1) which show the average fast wave polarization direction as trench-perpendicular (88.6°) and trench-parallel (8.5°), respectively. Both SMA and SC1 are classified as type II DSZs but they correspond to different circumstances. SMA is marked by Mariana-type slabs with large subduction angle and strong extension in back-arc, which is very different from SC1.

On the other hand, both TON and CA1 belong to type I DSZs, and they all have large angles of $|\phi_T - \phi|$ and subduction angle α_{DSZ}. They exhibit similar slab

morphologies but different slab kinematics. For example, we collected 12 seismic anisotropy data records in Tonga (TON) and obtained 64.3° of included angle between average fast wave polarization direction ϕ and trench strike ϕ_T, which is quite different with most of the type I DSZs. Recently, a so-called source-side splitting technique has been used to yield stronger constraints on the depth distribution of anisotropy beneath subducting slabs (e.g., Foley and Long 2011; Huang et al. 2011). With this method, they demonstrated that northern Tonga exhibits a well-developed pattern of trench-parallel polarization direction with a weak trend of decreasing δt with focal depth for upper mantle events. This kind of difference thus provides support for the interpretation that the splitting primarily reflects the complexity of seismic anisotropy along the depth distribution beneath the slab.

Many measurements of delay time δt between the fast and slow arrivals of shear wave have been used, especially in the noisy environments that characterize many stations in subduction settings. These methods are mainly used to extract splitting parameters from seismograms as accurately as possible when the δt is much smaller than the characteristic period of the shear wave (e.g., Vecsey et al. 2008; Wüstefeld et al. 2009). Although the well-constrained estimates of δt can be obtained from seismogram records, the complex patterns of seismic anisotropy along a splitting ray path can result in very complicated shear wave (e.g., Silver and Savage 1994; Long 2013; Mohiuddin et al. 2015). Additional complications arise as the splitting parameters are dependent on the frequency content of the shear wave (e.g., Wirth and Long 2010]. The propagation time for each segment of the splitting wave ray path is added to the total δt, which is probably the primary reason for inducing the relatively poor linear relationship between average δt and subduction angle α_{DSZ} (Fig. 5b). On the other hand, the average fast wave polarization direction is mainly dominated by the segment with the strongest seismic anisotropy on a splitting ray path. The part with very weak anisotropy generally decreases the degree of seismic anisotropy rather than changes the last polarization direction of the splitting wave. However, the average seismic anisotropy (δt, ϕ) we obtained in this study mainly represents the statistical mean results reflecting not only in vertical splitting wave ray paths beneath the station regions but also in horizontal area through the whole subduction zone.

In this study, we chose 39 subducting slabs along with the related information about DSZs. These slabs are mostly located around the Pacific Ocean (Fig. 2). However, we only collected approximately 500 seismic anisotropy data records. These records were less than what we expected and were distributed nonuniformly in these subduction zones. For example, these seismic anisotropy data are mainly concentrated in 24 subduction zones. If additional anisotropy data were gathered for the other 15 subduction zones (i.e., ME1, ME2, PE1, etc. in Fig. 2), the equations derived in this study will be more objective to reflect the correlations among seismic anisotropy and the other related parameters describing different types of DSZs. In addition to this, more detailed researches including geodynamical modeling constraints are also necessary to help us understand seismic anisotropy and DSZs' properties in subduction zones.

6.2 Average seismic anisotropy (δt, ϕ) and the weighted coefficient

In fact, these fast wave polarization direction data are from different studies accompanied by different qualities. Theoretically, the greater the quality of the data is, the larger the weighted coefficient should be when we add it to the oriented statistical analysis. Since we have filtered and removed those poor-quality data having a low signal-to-noise ratio, unclear waveform, and displaying nonelliptical particle motion (Schutt and Fouch 2001; Wüstefeld et al. 2009; Sun and Wei 2013), we use an equal weighting coefficient to all the remaining high-quality and fair-quality polarization data in this study.

The delay time is potentially another factor considered as a weighted coefficient in our analysis. In terms of two defined seismic ray paths with an equal propagation length, there is a positive correlation between the delay time and the degree of seismic anisotropy (e.g., Long 2013). We can therefore put a greater weighted coefficient to the data with larger delay time record. Assuming that there are n anisotropy indicators with the weighted coefficient $f_i = \delta t_i$ for the i-th indicator within a defined subduction zone, the corresponding value R, which is normalized to the range of 0 to 1, can be changed by Eqs. (3) and (4) as follows:

$$\bar{R} = \frac{1}{W}\sqrt{C^2 + S^2}, \tag{8}$$

where $W = \sum_{i=1}^{n} f_i$, $C = \sum_{i=1}^{n} f_i \cos \theta_i$, $S = \sum_{i=1}^{n} f_i \sin \theta_i$. We calculated the average fast wave polarization directions (ϕ) of the corresponding 20 DSZs that contain two or more anisotropy indicators (Table 1), which are listed in Table 2. In comparison with Table 1, we found that most directions change no more than 10°. The most prominent change is that the average polarization direction (107.3°) in NIZ (northern Izu of Japan) passes the Rayleigh test now and can be used in the linear regression. The subduction angle α_{DSZ} and the included angle $|\phi_T - \phi|$ for NIZ in this case are 58.6° and 31°, respectively. Using the least squares method, we calculated the linear equation as $|\phi_T - \phi| = -1.49\alpha_{DSZ} + 103.0$ without considering SC1,

Table 2 Weighted statistical analysis of the DSZs

Name	Number	$\bar{R}$	ϕ	Rayleigh test	ϕ_{APM}	$|\phi_{APM} - \phi|$	$|\phi_{T} - \phi|$
Kam1	1	–	33.0	1	304.7	88.3	13.0
SKUR	9	0.629	1.9	Pass	287.9	74.0	38.7
JAP	119	0.255	119.7	Pass	299.3	0.4	64.4
NIZ	40	0.301	107.3	Pass	292.9	5.6	58.6
KUR	1	–	1.0	1	288.0	73.0	34.0
SC1	9	0.648	12.8	Pass	75.2	62.4	6.7
NZ1	3	0.991	110.6	Pass	262.3	28.3	24.3
NZ2	12	0.322	33.2	–	72.3	39.1	35.6
NC1	30	0.431	65.0	Pass	72.3	7.4	69.9
CC1	13	0.870	79.7	Pass	71.6	8.1	79.7
CC2	17	0.764	101.5	Pass	272.3	9.2	58.5
JF1	21	0.808	65.3	Pass	52.9	12.4	80.6
JF2	126	0.710	70.1	Pass	12.3	57.9	80.1
WA1	2	0.443	76.5	–	360.0	76.5	68.6
SUM1	2	0.443	76.5	–	358.1	78.4	68.7
SUM2	1	–	168.0	1	2.8	14.8	23.1
JAV1	1	–	105.0	1	4.9	79.9	8.9
EA2	31	0.835	161.8	Pass	328.6	13.2	33.7
CA1	2	0.993	28.9	Pass	310.5	78.4	61.1
CA2	6	0.973	41.3	Pass	314.2	87.1	13.2
SIZ	12	0.211	103.5	–	292.6	9.1	66.6
SMA	15	0.873	131.7	Pass	293.3	18.5	88.0
TON	12	0.765	146.4	Pass	334.2	7.8	53.6
TW	39	0.410	26.5	Pass	304.1	82.4	63.5

$\bar{R}$ is the mean resultant length; ϕ is the mean direction; ϕ_{APM} is the direction of absolute plate motion; ϕ_{T} is the trench strike

In the column related to the Rayleigh test, "1" means one data in the DSZs, "Pass" means passing the Rayleigh test, and "–" means failing the Rayleigh test

SMA CA1, and TON as before. This agrees well with Eq. (5) in Sect. 5.

6.3 Seismic anisotropy and absolute plate motions

The statistical analysis method adopted in this study presumes that the observed vectors are sampled from a von Mises distribution. In this case, if the vectors were actually sampled from another type of distribution, the test would provide misleading results. Moreover, the statistical analysis method of directional data was used to study the overall reflection of seismic anisotropy in the research area. However, this method cannot highlight the area's local characteristics. In terms of the amount of data, seismic anisotropy data cannot cover all of the DSZs. The data distribute unevenly in the DSZs, which affects the statistical result. Another limitation of this study is that we did not consider an original signal for collecting data. We merely filtered available data and did not classify them. Data classification is necessary for a more detailed study in the future.

We use the absolute plate motion (APM) model to calculate plate motion and further compare it with the anisotropy, though the relevance between them is not definitely determined. In some subduction zones, such as the northeastern Japan, the fast wave polarization direction is likely related to the relative plate motion (Nakajima and Hasegawa 2004). Nevertheless, some previous studies have found that the seismic anisotropy is highly relevant to the APM of the Earth's surface areas, including the subduction zones, the mid-ocean ridge, and the interior of the continental plates (Debayle et al. 2005; Wang et al. 2008). Sun et al. (2013) conducted a statistical analysis to examine the relation among seismic anisotropy, plate motion, and stress orientations. Their results showed that APM is highly correlated with the seismic anisotropy in the interiors of the Arab, Caribbean, Juan de Fuca, North America, Nazca, the Pacific, and South America plates. However, the case of Africa, Antarctica, Australia, Europe, and Asia, including India and Philippine Sea, is weakly related to APM.

We use the APM model HS3-NUVEL-1A (Gripp and Gordon 2002) to determine the direction of subduction and the rate of the subducting plate. The APM directions of the 18 DSZs that contain seismic anisotropy data passing the Rayleigh test are listed in Table 2. These APM-related factors were also analyzed in relation to average delay time and average fast wave polarization direction. However, there is no obvious relationship between these APM-related
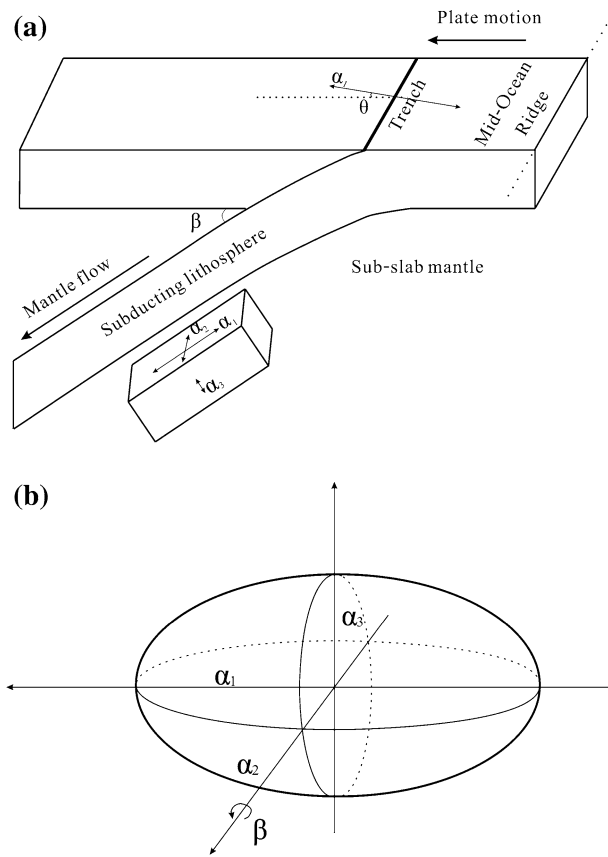
(a)

(b)

Fig. 6 Schematic of mechanism. **a** Schematic of seismic anisotropy in subduction. The three mutually orthogonal axes α_1, α_2, and α_3 represent the trench-perpendicular, trench-parallel, and the *vertical directions*, respectively, and $\alpha_1 > \alpha_2 > \alpha_3$. β is the subduction angle. **b** The corresponding Fresnel polarization ellipsoid

factors and average delay time or average fast wave polarization direction. For example, the included angle $|\phi_T - \phi|$ shows a random distribution with the included angle between the direction of absolute plate motion ϕ_{APM} and average fast wave polarization direction ϕ (Fig. 4b). This is somewhat different from the early theory of plate tectonics, in which the upper mantle flows should be consistent with the direction of plate convergence.

6.4 Olivine's LPO and a possible crystal description of the subducting oceanic lithosphere

DSZs' subduction angle, one of the important parameters for DSZs, not only describes the type of the subduction zone, but also reflects the different slab morphology. Complex slab morphology has also been invoked to explain the complex splitting patterns in subduction zone (Kneller and van Keken 2007). It is generally agreed that olivine's LPO makes the primary contribution to mantle anisotropy. High-pressure and high-temperature experiments have shown that many types of LPO in olivine can

be determined based on stress, pressure, temperature, and water content (Jung et al. 2006). Katayama and Karato (2006) studied the influence of temperature on the LPO of olivine and found that water-rich, low-stress, or high-temperature conditions produce type C LPO, whereas high-stress or low-temperature conditions produce type B LPO. The DSZ in northeastern Japan (JAP) satisfies the condition of type B LPO and is a cold subduction zone where an old plate is subducted. The DSZ in Juan de Fuca (JF1, JF2) is a warm subduction zone where a young plate is subducted and this DSZ satisfies the condition of type C LPO of olivine (Katayama and Karato 2006). Different types of LPO are often used to explain seismic anisotropy characteristics in subduction zones (e.g., Nakajima and Hasegawa 2004; Long and Silver 2008, 2009a, b).

Statistical results in Sect. 5.1 of this study showed that fast wave polarization direction changes gradually from trench-perpendicular to trench-parallel with the increase of subduction angle, which is similar to the results of Song and Kawakatsu (2012). In this study, we try to propose a possible crystal description of the subducting oceanic lithosphere to explain the above statistical results.

In Fig. 6a, we treat subducting oceanic lithosphere as a large crystal with three mutually orthogonal polarization direction, where the three axes α_1, α_2, and α_3 represent the trench-perpendicular, trench-parallel, and the *vertical*
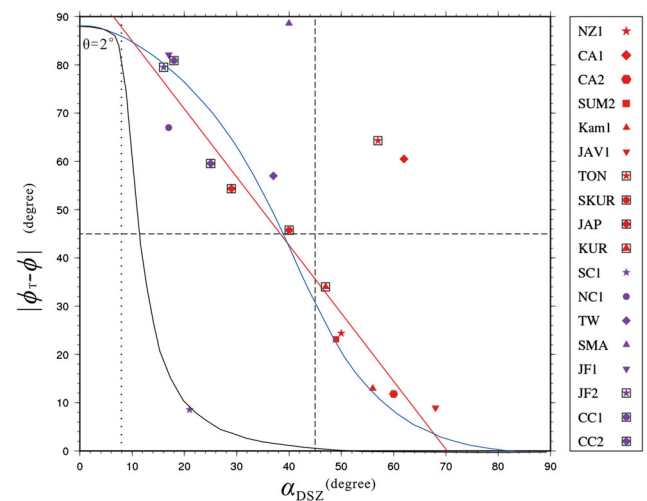

Fig. 7 Relationship between subduction angle and fast wave polarization direction. θ is the included angle between fast wave polarization direction (α_1) and normal direction of the trench strike; $|\phi_T - \phi|$ is the included angle between trench strike and average fast wave polarization direction; α_{DSZ} is the DSZs' subduction angle. *Black dotted l*ine indicates that $|\phi_T - \phi|$ changes with α_{DSZ} when θ is 0°; *Black line* indicates that $|\phi_T - \phi|$ changes with α_{DSZ} when θ is 2°; *blue line* indicates that $|\phi_T - \phi|$ changes with α_{DSZ} when θ is 2° after modifying the elastic constants ($c_{23} + 80, c_{13} + 53$). The *red line* indicates a linear fit to the data without considering SC1, SMA, TON, and CA1

Table 3 Modified elastic constants

C_{11}	C_{12}	C_{13}	C_{22}	C_{23}	C_{33}	C_{44}	C_{55}	C_{66}
320.5	68.1	124.6	196.5	156.8	233.5	64.0	77.0	78.7

The unit for elastic constants is GPa. Density is 3355.0 kg/m^3

directions, respectively. We consider it as a Fresnel polarization ellipsoid with three axes of α_1, α_2, and α_3 in Fig. 6b. In this case, the increase of subduction angle is equivalent to the Fresnel polarization ellipsoid rotating around the α_2 axis in the counterclockwise direction. We can thus obtain the velocity and polarization direction of the wave by solving the Christoffel equation (Musgrave 1970) when the elastic constants of the anisotropic crystal medium are known, and then calculate the relationship between subduction angle and fast wave polarization direction in the horizontal plane projection.

We are more concerned about the fast wave polarization direction in this study. Olivine, as the main mineral of the upper mantle, is generally most easy to deformation and orientation (Mao et al. 2015), which is often considered to be the main source of seismic anisotropy of this layer (e.g., Savage 1999). Therefore, we adopted olivine's elastic constants provided by Abramson et al. (1997) in calculation, which is similar that of Song and Kawakatsu (2012). Firstly, when α_1 axis is exactly along the trench-perpendicular direction, the theoretical included angle between fast wave polarization direction and trench strike jumps from 90° to 0° when the subduction angle is larger than about 8° (black dotted line in Fig. 7), which may be due to the symmetry of the elastic constants. Nevertheless, it is not consistent with the above statistical results that we obtained. So we let α_1 axis be slightly declined with $\theta = 2°$ from the trench-perpendicular direction (Fig. 6a). In this case, the corresponding calculated included angle between fast wave polarization direction and trench strike is not a jump but changes continuously from 90° to 0° with the increase of subduction angle, which is shown as black line in Fig. 7. We can find that it basically reflects the polarization rotation property of the Fresnel ellipsoid although it is quite different from the observed statistical results.

Furthermore, we tried to simulate the observed statistical results by modifying the elastic constants of the olivine crystal. We gave a well simulation model shown as blue line in Fig. 7 after a lot of tries, and the corresponding modified elastic constants are listed in Table 3.

The average fast wave polarization direction is mainly dominated by the oceanic lithosphere segment with the strongest seismic anisotropy on the entire splitting ray path as we discussed in Sect. 6.1, and the modified model describing the subducting oceanic lithosphere may reflect the mixture effect of olivine and other minerals, e.g., serpentine. If we considered the subducting oceanic lithosphere as the modified crystal model, the observed fast wave polarization direction corresponding to different subduction angles in subduction zones can be reasonably explained by rotating the oceanic lithosphere around the trench (or α_2 axis in Fig. 6) in the counterclockwise direction from 0° to 90°. In summary, the average fast wave polarization direction ϕ is strongly dependent on both the trench orientation ϕ_T and DSZs' subduction angle α_{DSZ} (see Eq. 5). When comparing to the previous Olivine's LPO theory, the Fresnel polarization ellipsoid model describing the subducting oceanic lithosphere in this study can provide a more reasonable explanation to the strong $|\phi_T - \phi|$ and α_{DSZ} correlation in DSZs.

References

Abramson EH, Brown JM, Slutsky LJ, Zaug J (1997) The elastic constants of San Carlos olivine to 17 GPa. J Geophys Res 102(B6):12253–12263. doi:10.1029/97JB00682

Anderson ML, Zandt G, Triep E, Fouch M, Beck S (2004) Anisotropy and mantle flow in the Chile-Argentina subduction zone from shear wave splitting analysis. Geophys Res Lett 31(23):L23608. doi:10.1029/2004gl020906

Ando M, Ishikawa Y, Yamazaki F (1983) Shear wave polarization anisotropy in the upper mantle beneath Honshu, Japan. J Geophys Res 88(B7):5850–5864

Anglin DK, Fouch MJ (2005) Seismic anisotropy in the Izu-Bonin subduction system. Geophys Res Lett 32(9):L09307

Barruol G, Hoffmann R (1999) Upper mantle anisotropy beneath the Geoscope stations. J Geophys Res 104(B5):10757–10773. doi:10.1029/1999jb900033

Bastowa ID, Juliàb J, Nascimento AF, Fuck RA, Buckthorp TL, McClellan JJ (2015) Upper mantle anisotropy of the Borborema Province, NE Brazil: implications for intra-plate deformation and sub-cratonic asthenospheric flow. Tectonophysics 657(30):81–93. doi:10.1016/j.tecto.2015.06.024

Bezacier L, Reynard B, Bass JD, Sanchez-Valle C, Van de Moortèle B (2010) Elasticity of antigorite, seismic detection of serpentinites, and anisotropy in subduction zones. Earth Planet Sci Lett 289(1–2):198–208

Bock G, Kind R, Rudloff A, Asch G (1998) Shear wave anisotropy in the upper mantle beneath the Nazca Plate in northern Chile. J Geophys Res 103(B10):24333–24345. doi:10.1029/98jb01465

Bonnin M, Barruol G, Bokelmann GHR (2010) Upper mantle deformation beneath the North American-Pacific plate boundary in California from SKS splitting. J Geophys Res 115(B4):B04306. doi:10.1029/2009jb006438

Bostock MG, Cassidy JF (1995) Variations in SKS splitting across western Canada. Geophys Res Lett 22(1):5–8

Boudier F, Baronnet A, Mainprice D (2010) Serpentine mineral replacements of natural olivine and their seismic implications: oceanic lizardite versus subduction-related antigorite. J Petrol 51(1–2):495–512

Bowman JR, Ando M (1987) Shear-wave splitting in the upper-mantle wedge above the Tonga subduction zone. Geophys J R Astron Soc 88(1):25–41

Brudzinski M, Thurber CH, Hacker BR, Engdahl ER (2007) Global prevalence of double Benioff zones. Science 316:1472–1474

Coblentz DD, Richardson RM (1995) Statistical trends in the intraplate stress field. J Geophys Res 100(B10):20245–20255. doi:10.1029/95JB02160

Currie CA, Cassidy JF, Hyndman RD, Bostock MG (2004) Shear wave anisotropy beneath the Cascadia subduction zone and western North American craton. Geophys J Int 157(1):341–353

Davis JC (1986) Statistics and data analysis in geology, 2nd edn. Wiley, New York

Debayle E, Kennett B, Priestley K (2005) Global azimuthal seismic anisotropy and the unique plate-motion deformation of Australia. Nature 433(7025):509–512

Eakin CM, Obrebski M, Allen RM, Boyarko DC, Brudzinski MR, Porritt R (2010) Seismic anisotropy beneath Cascadia and the Mendocino triple junction: interaction of the subducting slab with mantle flow. Earth Planet Sci Lett 297(3–4):627–632

Evans MS, Kendall JM, Willemann RJ (2006) Automated SKS splitting and upper-mantle anisotropy beneath Canadian seismic stations. Geophys J Int 165(3):931–942. doi:10.1111/j.1365-246X.2006.02973.x

Faccenda M, Burlini L, Gerya TV, Mainprice D (2008) Fault-induced seismic anisotropy by hydration in subducting oceanic plates. Nature 455(7216):1097–1100

Foley BJ, Long MD (2011) Upper and mid-mantle anisotropy beneath the Tonga slab. Geophys Res Lett 38(2):L02303. doi:10.1029/2010GL046021

Fouch MJ, Fischer KM (1996) Mantle anisotropy beneath northwest Pacific subduction zones. J Geophys Res 101(B7):15987–16002. doi:10.1029/96jb00881

Fouch MJ, Fischer KM (1998) Shear wave anisotropy in the Mariana Subduction Zone. Geophys Res Lett 25(8):1221–1224. doi:10.1029/98gl00650

Gripp AE, Gordon RG (2002) Young tracks of hotspots and current plate velocities. Geophys J Int 150(2):321–361

Hacker BR, Peacock SM, Abers GA, Holloway SD (2003) Subduction factory 2. Are intermediate-depth earthquakes in subducting slabs linked to metamorphic dehydration reactions? J Geophys Res 108(B1):2030. doi:10.1029/2001JB001129

Hammond J, Wookey J, Kaneshima S, Inoue H, Yamashina T, Harjadi P (2010) Systematic variation in anisotropy beneath the mantle wedge in the Java-Sumatra subduction system from shear-wave splitting. Phys Earth Planet Inter 178(3–4):189–201

Hanna J, Long MD (2012) SKS splitting beneath Alaska: regional variability and implications for subduction processes at a slab edge. Tectonophysics 530–531(2):272–285. doi:10.1016/j.tecto.2012.01.003

Hasegawa A, Umino N, Takagi A (1978) Double-planed deep seismic zone and upper-mantle structure in the Northeastern Japan Arc. Geophys J R Astr Soc 54(2):281–296

Hasegawa A, Horiuchi S, Umino N (1994) Seismic structure of the northeastern Japan convergent margin: a synthesis. J Geophys Res 99(B11):22295–22311. doi:10.1029/93JB02797

Hiramatsu Y, Ando M, Ishikawa Y (1997) ScS wave splitting of deep earthquakes around Japan. Geophys J Int 128(2):409–424

Huang ZC, Zhao DP, Wang LS (2011) Frequency-dependent shear-wave splitting and multilayer anisotropy in northeast Japan. Geophys Res Lett 38(8):L08302. doi:10.1029/2011GL046804

Igarashi T, Matsuzawa T, Umino N, Hasegawa A (2001) Spatial distribution of focal mechanisms for interplate and intraplate earthquakes associated with the subducting Pacific plate beneath the northeastern Japan arc: a triple-Planed deep seismic zone. J Geophys Res 106:2177–2191

Iidaka T, Obara K (1995) Shear-wave polarization anisotropy in the mantle wedge above the subducting Pacific plate. Tectonophysics 249(1–2):53–68

Jung H, Katayama I, Jiang Z, Hiraga T, Karato S (2006) Effect of water and stress on the lattice-preferred orientation of olivine. Tectonophysics 421(1–2):1–22. doi:10.1016/j.tecto.2006.02.011

Kaneshima S, Silver PG (1995) Anisotropic loci in the mantle beneath central Peru. Phys Earth Planet Inter 88(3–4):257–272

Kao H, Rau RJ (1999) Detailed structures of the subducted Philippine Sea plate beneath northeast Taiwan: a new type of double seismic zone. J Geophys Res 104(B1):1015–1033

Katayama I, Karato SI (2006) Effect of temperature on the B- to C-type olivine fabric transition and implication for flow pattern in subduction zones. Phys Earth Planet Inter 157(1–2):33–45. doi:10.1016/j.pepi.2006.03.005

Kawakatsu H (1986a) Double seismic zones: kinematics. J Geophys Res 91(B5):4811–4825

Kawakatsu H (1986b) Downdip tensional earthquakes beneath the tonga arc: a double seismic zone? J Geophys Res 91(B6):6432–6440

Kawakatsu H, Seno T (1983) Triple seismic zone and the regional variation of seismicity along the northern Honshu arc. J Geophys Res 88:4215–4230

Kneller EA, van Keken PE (2007) Trench-parallel flow and seismic anisotropy in the Mariana and Andean subduction systems. Nature 450(7173):1222–1225

Kuo-Chen H, Wu FT, Okaya D, Huang BS, Liang WT (2009) SKS/SKKS splitting and Taiwan orogeny. Geophys Res Lett 36(12):L12303. doi:10.1029/2009gl038148

Lallemand S, Heuret A, Boutelier D (2005) On the relationships between slab dip, back-arc stress, upper plate absolute motion, and crustal nature in subduction zones. Geochem Geophys Geosyst 6(9):Q09006. doi:10.1029/2005GC000917

Liu KH, Gao SS, Gao Y, Wu J (2008) Shear wave splitting and mantle flow associated with the deflected Pacific slab beneath northeast Asia. J Geophys Res 113(B1):B01305. doi:10.1029/2007jb005178

Long MD (2013) Constraints on subduction geodynamics from seismic anisotropy. Rev Geophys 51(1):76–112. doi:10.1002/rog.20008

Long MD, Becker TW (2010) Mantle dynamics and seismic anisotropy. Earth Planet Sci Lett 297(3–4):341–354

Long MD, Silver PG (2008) The subduction zone flow field from seismic anisotropy: a global view. Science 319(5861):315–318

Long M, Silver P (2009a) Shear wave splitting and mantle anisotropy: measurements, interpretations, and new directions. Surv Geophys 30(4–5):407–461. doi:10.1007/s10712-009-9075-1

Long MD, Silver PG (2009b) Mantle flow in subduction systems: the subslab flow field and implications for mantle dynamics. J Geophys Res 114(B10):B10312. doi:10.1029/2008JB006200

Long MD, van der Hilst RD (2005) Upper mantle anisotropy beneath Japan from shear wave splitting. Phys Earth Planet Inter 151(3–4):206–222

Long MD, van der Hilst RD (2006) Shear wave splitting from local events beneath the Ryukyu arc: trench-parallel anisotropy in the mantle wedge. Phys Earth Planet Inter 155(3–4):300–312

Long MD, Wirth EA (2013) Mantle flow in subduction systems: the mantle wedge flow field and implications for wedge processes. J Geophys Res 118(2):583–606. doi:10.1002/jgrb.50063

Long MD, Gao H, Klaus A, Wagner LS, Fouch MJ, James DE, Humphreys E (2009) Shear wave splitting and the pattern of mantle flow beneath eastern Oregon. Earth Planet Sci Lett 288(3–4):359–369. doi:10.1016/j.epsl.2009.09.039

Mao Z, Fan DW, Lin JF, Yang J, Tkachev SN, Zhuravlev K, Prakapenka VB (2015) Elasticity of single-crystal olivine at high pressures and temperatures. Earth Planet Sci Lett 426(15):204–215. doi:10.1016/j.epsl.2015.06.045

Mardia KV (1972) Statistics of directional data. Academic Press, London

Meade C, Silver PG, Kaneshima S (1995) Laboratory and seismological observations of lower mantle isotropy. Geophys Res Lett 22(10):1293–1296

Mohiuddin A, Long MD, Lynner C (2015) Mid-mantle seismic anisotropy beneath southwestern Pacific subduction systems and implications for mid-mantle deformation. Phys Earth Planet Inter 245:1–14. doi:10.1016/j.pepi.2015.05.003

Monteiller V, Chevrot S (2011) High-resolution imaging of the deep anisotropic structure of the San Andreas Fault system beneath southern California. Geophys J Int 186(2):418–446. doi:10.1111/j.1365-246X.2011.05082.x

Musgrave MJP (1970) Crystal acoustics. Holden-Day, San Francisco

Nakajima J, Hasegawa A (2004) Shear-wave polarization anisotropy and subduction-induced flow in the mantle wedge of northeastern Japan. Earth Planet Sci Lett 225(3–4):365–377

Nakajima J, Shimizu J, Hori S, Hasegawa A (2006) Shear-wave splitting beneath the southwestern Kurile arc and northeastern Japan arc: a new insight into mantle return flow. Geophys Res Lett 33(5):L05305

Ohmi S, Hori S (2000) Seismic wave conversion near the upper boundary of the Pacific plate beneath the Kanto district, Japan. Geophys J Int 141(1):136–148

Özalaybey S, Savage MK (1995) Shear-wave splitting beneath western United States in relation to plate tectonics. J Geophys Res 100(B9):18135–18149

Peacock SM (2001) Are the lower planes of double seismic zones caused by serpentine dehydration in subducting oceanic mantle? Geology 29(4):299–302

Peyton V, Levin V, Park J, Brandon M, Lees J, Gordeev E, Ozerov A (2001) Mantle flow at a slab edge: seismic anisotropy in the Kamchatka region. Geophys Res Lett 28(2):379–382

Polet J, Silver PG, Beck S, Wallace T, Zandt G, Ruppert S, Kind R, Rudloff A (2000) Shear wave anisotropy beneath the Andes from the BANJO, SEDA, and PISCO experiments. J Geophys Res 105(B3):6287–6304

Russo RM, Silver PG (1994) Trench-Parallel flow beneath the Nazca plate from seismic anisotropy. Science 263(5150):1105–1111. doi:10.1126/science.263.5150.1105

Russo RM, Silver PG (1996) Cordillera formation, mantle dynamics, and the Wilson cycle. Geology 24(6):511–514. doi:10.1130/0091-7613

Savage M (1999) Seismic anisotropy and mantle deformation: what have we learned from shear wave splitting. Rev Geophys 37(1):65–106

Schutt D, Fouch M (2001) http://geophysics.aus.edu/anisotropy/upper/index.html

Silver PG (1996) Seismic anisotropy beneath the continents: probing the depths of geology. Annu Rev Earth Planet Sci 24:385–432

Silver PG, Chan WW (1988) Implications for continental structure and evolution from seismic anisotropy. Nature 335(1):34–39

Silver PG, Chan WW (1991) Shear wave splitting and subcontinental mantle deformation. J Geophys Res 96(B10):16429–16454. doi:10.1029/91jb00899

Silver PG, Savage MK (1994) The interpretation of shear-wave splitting parameters in the presence of two anisotropic layers. Geophys J Int 119(3):949–963

Song TRA, Kawakatsu H (2012) Subduction of oceanic asthenosphere: evidence from sub-slab seismic anisotropy. Geophys Res Lett 39(17):L17301. doi:10.1029/2012GL052639

Stern RJ (2002) Subduction zones. Rev Geophys 40(4):1012–1049. doi:10.1029/2001RG000108

Sun ZT, Wei DP (2013) Compilation of the global seismic aniosotropy data and review of related researches. Prog Geophys 28(3):1280–1288

Sun ZT, Wei DP, Han P, Liu L (2013) Statistical analysis on the correlation between plate motion and seismic anisotropy as well as stress field. Acta Seismol Sin 35(6):785–798

Sykes LR (1966) The seismicity and deep structure of island arcs. J Geophys Res 71(12):2981–3006

Teng JW, Zhang YQ, Ruan XM (2012) The seismic anisotropy of the crustal and mantle medium of the Earth interior and its dynamical respond. Chinese J Geophys 55(11):3648–3670

Uyeda S, Kanamori H (1979) Back-arc opening and the mode of subduction. J Geophys Res: Solid Earth 84(B3):1049–1061. doi:10.1029/JB084iB03p01049

Vecsey L, Plomerová J, Babuška V (2008) Shear-wave splitting measurements—problems and solutions. Tectonophysics 462(1–4):178–196. doi:10.1016/j.tecto.2008.01.021

Vinnik LP, Makeyeva LI, Milev A, Usenko AY (1992) Global patterns of azimuthal anisotropy and deformations in the continental mantle. Geophys J Int 111(3):433–447. doi:10.1111/j.1365-246X.1992.tb02102.x

Wang CY, Flesch LM, Silver PG, Chang LJ, Chan WW (2008) Evidence for mechanically coupled lithosphere in central Asia and resulting implications. Geology 36(5):363–366

West JD, Fouch MJ, Roth JB, Elkins-Tanton LT (2009) Vertical mantle flow associated with a lithospheric drip beneath the Great Basin. Nat Geosci 2(6):439–444

Wirth E, Long MD (2010) Frequency-dependent shear wave splitting beneath the Japan and Izu-Bonin subduction zones. Phys Earth Planet Inter 181(3–4):141–154. doi:10.1016/j.pepi.2010.05.006

Wookey J, Kendall JM, Barruol G (2002) Mid-mantle deformation inferred from seismic anisotropy. Nature 415(6873):777–780

Wüstefeld A, Bokelmann G, Barruol G, Montagner JP (2009) Identifying global seismic anisotropy patterns by correlating shear-wave splitting and surface-wave data. Phys Earth Planet Inter 176(3–4):198–212. doi:10.1016/j.pepi.2009.05.006

Yamasaki T, Seno T (2003) Double seismic zone and dehydration embrittlement of the subducting slab. J Geophys Res 108(B4):2212–2232

Zhang ZJ (2002) A review of the seismic anisotropy and its applications. Prog Geophys 17(2):281–293 **(in Chinese with English abstract)**

Zhang KL (2010) Characteristic analysis of double seismic zones and numerical simulation on the thermal structure of subduction zones. Phd Thesis, Graduate University of the Chinese Academy of Sciences, Beijing

Zhang KL, Wei DP (2008) Progresses of the researches and the causing mechanisms on the double seismic zones within the subduction zones around the pacific ocean. Prog Geophys 23(1):31–39 **(in Chinese with English abstract)**

Zhang KL, Wei DP (2011) On the influence factors of double seismic zones. Chinese J Geophys 54(11):2838–2850 **(in Chinese with English abstract)**

Zhang KL, Wei DP (2012) Correlation between plate age and layer separation of double seismic zones. Earthq Sci 25(1):95–101. doi:10.1007/s11589-012-0835-5